Reef influence quantification in light of the 1771 Meiwa tsunami

Ocean and Coastal Management 195 (2020) 105248

Contents lists available at ScienceDirect

Ocean and Coastal Management

journal homepage: http://www.elsevier.com/locate/ocecoaman

Reef influence quantification in light of the 1771 Meiwa tsunami

Marine Le Gal *, Satoshi Mitarai

Marine Biophysics Unit, Okinawa Institute of Science and Technology Graduate University, 1919-1 Tancha, Onna-son, Kunigami-gun, Okinawa, 904-0495, Japan

ARTICLE INFO

Keywords:
Tsunamis
Reef
Meiwa 1771
Non-linear shallow water models

ABSTRACT

While interactions between regular wave driven flooding and reefs have been widely studied due to climate change pressure, the effects of reefs on tsunami flooding have less been investigated. From studies of historical events, reefs can behave as buffers or as amplifiers of inundation, depending upon the location. Interactions between reefs and tsunamis have generally been analyzed with idealized models, and there have been only few studies of specific reefs and their characteristics. Using numerical NonLinear Shallow Water models, this study characterizes the influence of the Southeast Ishigaki Island reef during the 1771 tsunami that hit the Yaeyama Islands. In this work, we modified reef topography *in silico* and then, measured the impact of these changes using a new parameter, the Reef Impact Factor (RIF). First, a reference model was built, simulating the real event with an accurate reef representation and using run-up data to calibrate bottom friction. This calibration highlights the difficulty of representing reef friction with a homogeneous coefficient. Second, a model without a reef was compared to the reference model. The impact of reef removal varies considerably along the coastline and maximum wave heights at the shore were strongly affected, with a 12.5% increase on average. Overall, this suggests a protective role of the reef along most of the coast. However, at local scale, channels that break the continuity of the front reef, increased wave heights by up to 40% on the proximate coast, revealing their strong focusing influence. Finally, changes in tide level, which regulates reef depth, were investigated, showing a global positive correlation between sea level and maximum wave height at the coast. However, the impact of the reef depth appeared weak compared to the impact of incident wave parameters. This study contributes to a global effort to understand tsunami-reef interactions in a non-idealized framework, suggesting a Reef Impact Factor for inter-reef/study comparisons. Moreover, vulnerable and exposed coasts were identified at Ishigaki Island, which may help to improve inundation forecasting, resulting in more appropriate management of these vulnerable sections of the coast.

1. Introduction

Due to concerns about sea level increases, more frequent typhoons, and increasing human populations in coastal areas, the influence of reefs on non-tsunami wave-driven flooding (regular flooding in the following) have been well investigated (Ferrario et al., 2014; Storlazzi, 2018; Quataert et al., 2015; Tajima et al., 2016; Péquignet et al., 2011; Pearson et al., 2017). Ferrario et al. (2014) estimated that, in general, reefs reduce wave energy by more than 80%, as long as no resonance phenomena are occurring (only 3.5% of the waves according to Gawehn et al. (2016), Péquignet et al. (2009); Pearson et al. (2017). However, previous studies have not examined the roles of reefs during tsunami inundations, for which the wave parameters differ from those considered, while they have proven important (Lynett, 2007). One of the major difference is the wave period, usually under 20 s for storm waves and larger than a minute for tsunami waves, Liu (2009). While reefs are generally assumed to function as buffers during tsunami events (Lynett, 2007; Baba et al., 2008), it has been shown that in certain situations, reefs can exacerbate inundation (Baird et al., 2005; Roeber et al., 2010; Dilmen et al., 2018). Numerous experimental and numerical studies have addressed this question using one- (Kunkel et al., 2006; Shao et al., 2019; Yao et al., 2018) or two- (Roger et al., 2014; Gelfenbaum et al., 2011) dimensional models of idealized reefs. The impact of reefs on waves is twofold. On one hand they modify bottom friction (usually by increasing it), which attenuates in-coming surface waves, and on the other hand, reef morphology and structure, that impact shoaling, resonance, and refractive effects, can induce more severe localized inundations (Gelfenbaum et al., 2011). Reef roughness was considered the most important parameter by Gelfenbaum et al. (2011), while others have suggested that reef depth has a greater impact (Yao et al., 2018;

* Corresponding author.
E-mail address: marine.legal@oist.jp (M. Le Gal).

https://doi.org/10.1016/j.ocecoaman.2020.105248
Received 13 December 2019; Received in revised form 26 April 2020; Accepted 29 April 2020
Available online 6 July 2020

Shao et al., 2019). Using a numerical Nonlinear Shallow Water model for an idealized reef, Kunkel et al. (2006) identified key parameters, including the depth and width of the reef and the width of the lagoon behind the reef, which has also been identified by Roger et al. (2014) as a crucial parameter. Another important feature is the presence of gaps or channels in the reef (Fernando et al., 2005; Kunkel et al., 2006; Gelfenbaum et al., 2011). These gaps reduce reef effectiveness, leading to more severe local inundations of the coast.

To our knowledge, and given the aforementioned complexity, studies that have investigated specific reefs and their influence upon tsunamis are rare. For instance, Tutuila Island was studied several times following a 2009 event (Roeber et al., 2010; Gelfenbaum et al., 2011; Dilmen et al., 2018). Dilmen et al. (2018) used a 2D numerical model to represent the 2009 Samoa tsunami that hit Tutuila island. By changing the Manning coefficient, which regulates bottom friction, they demonstrated how spatially complex the roughness representation can be and the difficulty in attempting to represent it with a uniform coefficient. Moreover, by modifying the smoothness of grid bathymetry, they highlighted the strong impact of local bathymetry on inundation, with occasional amplification of flooding due to the reef. Similarly, Baba et al. (2008) used a smoothing effect in a numerical model of the 2007 Solomon Island tsunami to measure the influence of the Great Barrier Reef in Australia. They concluded that the reef had a protective effect. In their work, Miyazawa et al. (2012) re-evaluated the model of Imamura (2001) of the 1771 Yaeyama tsunami using a finer bathymetry dataset with a better reef representation. The authors observed a decrease in the resulting run-up, suggesting attenuation by the reef. However, the authors compared results from two different bathymetry datasets, inducing different coastline and shore topographies that together with the reef representation, contribute to the inundation process and impact run-up values. In the present study, we have attempted a deeper and more quantitative analysis. The same bathymetry dataset (shore topography) was used for all simulations and only the reef area was modified for the purpose of the present study.

The present work determines the role of the reef along the southeast coast of Ishigaki Island (Japan) during the 1771 Yaeyama tsunami. Extremely high run-ups occurred during this event (Goto et al., 2010), especially at Ishigaki Island, which, like many other Pacific islands, is characterized by an irregular coastline with a reef. The recurrence interval of events of this magnitude has been estimated at 150− 400 years (Araoka et al., 2013). The frequency of this hazard may be lower than that of regular flooding (7.4 typhoons per year estimated by Hongo et al. (2012) in Ryukyu Islands), but tsunami waves can be more powerful and destructive. Although typhoons may have a greater accumulated total energy, one single tsunami wave is more energetic (Weiss, 2012). Better understanding of the hydrodynamic processes of this event will allow better forecasting of what could happen in the future, leading to improved coastal management. Following the lead of Baba et al. (2008) and Dilmen et al. (2018), this study contributes to the effort to understand tsunami-reef interactions in a non-idealized scenario.

For this study, a numerical model of the event using the Nonlinear Shallow Water model was developed, and in order to measure the impact of the reef, a Reef Impact Factor is defined. Methods are described Section 2, and the Meiwa tsunami is briefly presented in Section 3. First, in Section 4.1, this model is calibrated against data (Goto et al., 2010) by testing different friction coefficients. Second, in Section 4.2, the role of the reef is addressed by modifying the bathymetry. The reef was erased from the grid to measure the difference in the inundation with and without it. Finally, the impact of reef depth was investigated in Section 4.3. The numerical results are analyzed and discussed in Section 5.

2. Methods

2.1. Hydrodynamic model

This study was performed using the Nonlinear Shallow Water Telemac2D model (Opentelemac (Accessed April 8, 2020), Hervouet (2007)). The following equations are solved for water depth $h(m)$ and depth-averaged velocity $\overrightarrow{u} = (u, v)(m.s^{-1})$:

$$\begin{cases} \dfrac{\partial h}{\partial t} + \overrightarrow{u}.\nabla h + h(\nabla.\overrightarrow{u}) = S_h \\ \dfrac{\partial u}{\partial t} + \overrightarrow{u}.\nabla u = -g\dfrac{\partial Z}{\partial x} + S_x + \dfrac{1}{h}\nabla.(h\nu\nabla u) \\ \dfrac{\partial v}{\partial t} + \overrightarrow{u}.\nabla v = -g\dfrac{\partial Z}{\partial y} + S_y + \dfrac{1}{h}\nabla.(h\nu\nabla v) \end{cases} \quad (1)$$

with $t(s)$ the time, $g(m.s^{-2})$ the gravity acceleration, $\nu(m^2.s^{-1})$ the momentum diffusion coefficient, $S_h(m.s^{-1})$, $S_x, S_y(m.s^{-2})$ source or sink terms, and $\eta(m)$ the free surface elevation.

For real case events, the Coriolis force and bottom friction are added in the definition of S_x and S_y. The Coriolis force is calculated as:

$$\overrightarrow{F_{cor}} = 2\omega\sin\lambda\,\overrightarrow{u},$$

with ω the angular velocity of the Earth and λ the latitude of the considered grid node. For bottom friction, the bottom shear stress is represented as:

$$\overrightarrow{\tau} = -\frac{1}{2}\rho C_D|\overrightarrow{u}|\overrightarrow{u},$$

with ρ the density and C_D a dimensionless friction coefficient. In the present study, the Strickler law (Strickler, 1981) was chosen to represent C_D :

$$C_D = \frac{2g}{h^{\frac{1}{3}}S^2} \quad (2)$$

with $S\ (m^{1/3}.s^{-1})$ the coefficient of Strickler, in which a lower coefficient represents greater friction. The choice of the Strickler coefficient is addressed in Section 4.1.

Telemac2D has been tested and validated for tsunami modelling through test cases by Violeau et al. (2016) and used for real tsunami events by Horsburgh et al. (2008), Grilli et al. (2016), Le Gal et al. (2018), Williams et al. (2019) among others.

2.2. Bathymetry and mesh

The present numerical model focuses on the hydrodynamics along Ishigaki Island coast and reef. Integrating the reef in the mesh bathymetry was critical. To this end, the mesh along the coastline and inside the reef parts must be precisely defined in order to give an accurate representation of these areas. Generation of the mesh was carried out using Blue Kenue software (NRC, 2010). To create the mesh and its bathymetry, four bathymetry databases were used, depending on the area:

- Open ocean: SRTM 15' (Becker et al., 2009)
- Coast: M5000 serie (until 1010 m of resolution, JHA et al. (2016))
- Inner reef part: Satellite Database Landsat 8 (Roy et al., 2014), transformed using the software BathyMapper (resolution ~30m).
- Inside ground land: SRTM 90 m (Jarvis et al., 2008).

To convert the Landaset 8 dataset, BathyMapper (JHA, 2016) uses the Lyzenga Model (Lyzenga et al., 2006), and a bathymetry measurement shown in Suzuki (2005) as a reference for calibration. A comparison between the output bathymetry data grid and the reference is shown in Fig. 1. Being able to accurately represent the reef around Ishigaki allowed us to draw conclusions fitting the Ishigaki shore;

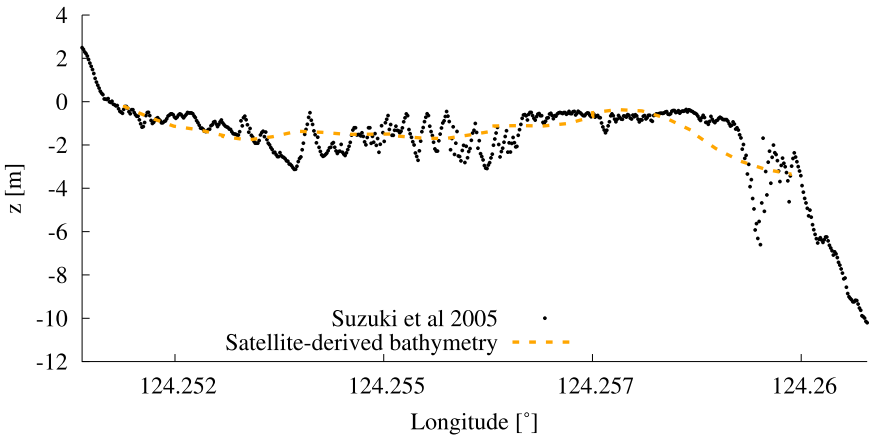

Fig. 1. Comparison of bathymetry measurements from Suzuki (2005) and the satellite-derived bathymetry grid obtained from Landsat 8 (Roy et al., 2014) and BathyMapper (JHA, 2016), represented by black points and the orange dashed line, respectively. (For interpretation of the references to color in this figure legend, the reader is referred to the Web version of this article.)

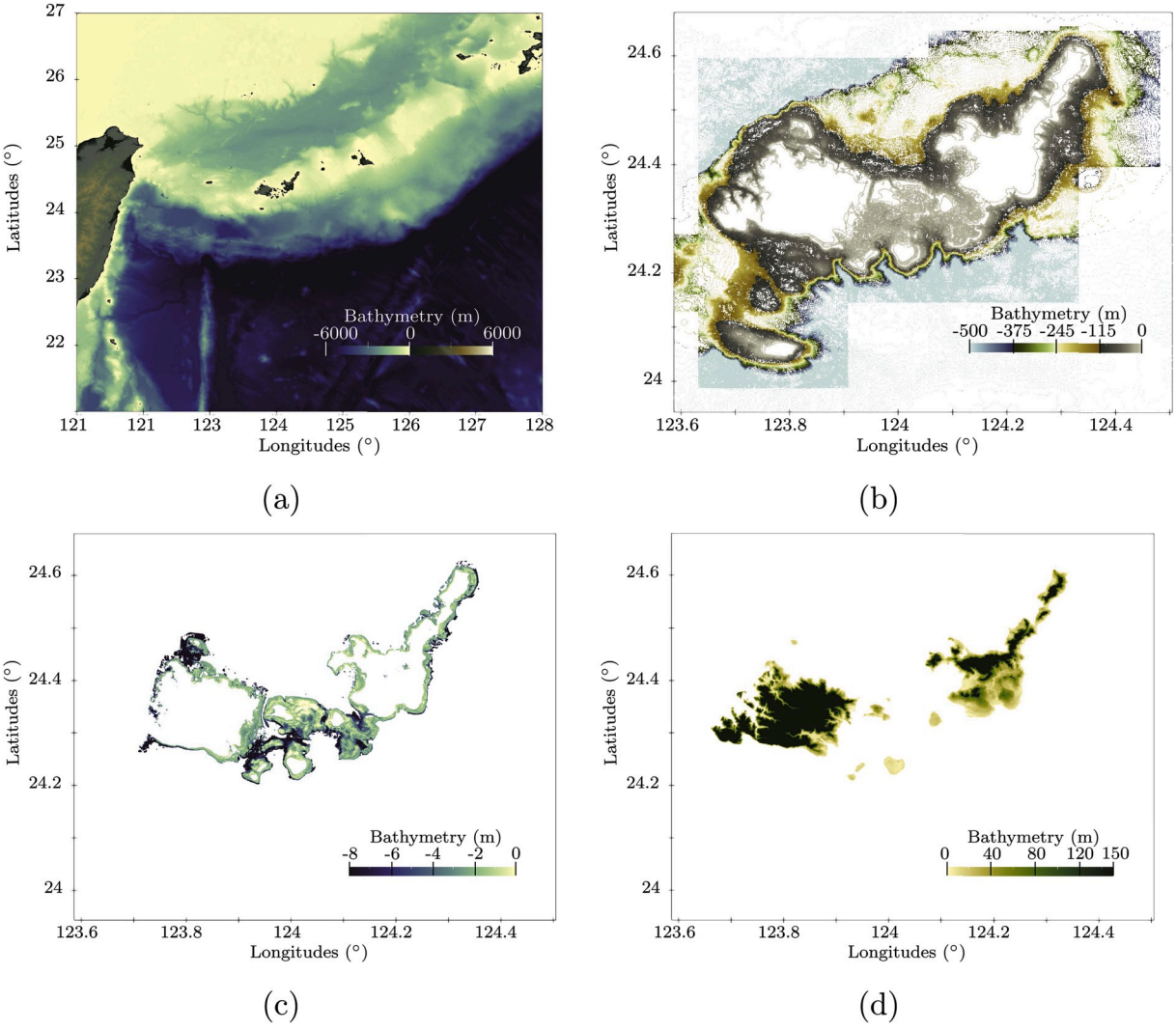

Fig. 2. Distribution of the databases used. (2a) SRTM 15' and JHA contourline databases were used for open ocean and coastal zones, respectively. The black rectangle is the limit of the zoom on Ishigaki and Iriomote Islands (Captions 2b, 2c, 2d). (2b) JHA contour database for the coastal area. (2c) Satellite-derived bathymetry created for the present study of the inner reef area. (2d) SRTM 90 m database for inner island grounds. The color scale range changes at each sub-caption. (For interpretation of the references to color in this figure legend, the reader is referred to the Web version of this article.)

however, the aim of this work was not to focus on a perfect reproduction of reef bathymetry in the model grid.

Local depth determines the size of the cells. Using the SRTM 15' database, a 1,800,000 node mesh was created with cell sizes between 20 m at the coast and 10 km in the open ocean. Bathymetry databases were interpolated using an inverse distance method in their respective areas. Distributions of the databases in the domain are shown in Fig. 2. The final mesh and associated bathymetry are represented in Fig. 3.

2.3. Reef Impact Factor

Run-up represents one aspect of inundation and depends on numerous parameters, such as wave linearity and height, topography of the shore, and bottom friction. Modelling the inundation process on land would add more approximations to calculations. To avoid this, the present analysis is based on the maximum water depth at the coastline (MWDC), equivalent to the maximum wave height at the same location (Fig. 4).

The relationship between run-up and offshore wave height was studied by Synolakis (1991) and others, showing a positive, but nonlinear correlation between these two variables. In consequence, all quantifying results given in this study refer to the maximum water depth, and we assume that inundation qualitatively follows the same trends. For the sake of clarity, the Reef Impact Factor (RIF), a ratio normalizing the result obtained from a modified reef model by a reference model (real reef model, see Section 4.1) is defined as:

$$RIF = \left(\frac{(\text{MWDC modified reef model})}{(\text{MWDC reference model})} - 1.0 \right) \times 100. \quad (3)$$

The multiplying factor 100 makes RIF a percentage. The RIF indicates the impact of reef modification on the MWDC. If the RIF is negative, the wave at the shore is smaller for the modified reef model, suggesting that changes made to the reef led to a reduction of wave heights. If the RIF is positive, the changes led to an amplification of the wave. Previously, mainly qualitative analyses were presented to explain reef influence (Baba et al., 2008; Dilmen et al., 2018). The advantage of the RIF is that it allows comparisons between reef studies, idealized or not, since shore topography is not considered. It also easily and clearly quantifies the impact of any given reef. Similar indicators have been used to assess reef impact. For instance Costa et al. (2016) worked with a wave transmission coefficient for a regular swell above the Northeast Bresilian reef. However, the measurement locations in this study depended upon the reef geometry. Klaver et al. (2019) investigated the impact of a pit in an idealized reef, using similar wave height normalisation along with variance of density spectra. In this study, wave height was assessed at the beach-toe, the location of which is easily recognizable in an idealized model, but less easy to identify in a real system. For reef-tsunami interactions, Gelfenbaum et al. (2011) also worked with the maximum wave height at the shoreline relative to no reef (equivalent to RIF), in addition to inundation distance and maximum velocity at the shoreline. The authors used these normalisations as indicators of the impact of different reef geometry parameters in a one-dimensional idealized analysis, and to assess the impact of idealized channels and embayments. This equivalence allowed us to compare the present outputs with those of Gelfenbaum et al. (2011), see below.

3. The 1771 Meiwa tsunami

On April 24, 1771, a tsunami hit the Yaeyama islands (Ryukyu Archipelago, Japan). The source of this tsunami is still uncertain, but its intensity is evident from the numerous boulders found along the coastline. Studies based on geological and historical data have been published by Nakata and Kawana (1995) and Goto et al. (2010) among others. In the latter work, the authors gathered information about run-up heights and estimated a probable maximum run-up height close to 32 m at Miyara, Ishigaki Island. The number of victims for this event is estimated around ~12,000 people (approximately 48% of the island's population (Goto et al., 2010)).

Uncertainty regarding the source of the tsunami has led to numerous generation models, which are still under debate. Different kinds of generation have been suggested: a unique fault model (Nakamura, 2009), one fault plus a landslide model (Imamura, 2001) or two faults and a landslide model (Miyazawa et al., 2012), among others.

Miyazawa et al. (2012) compared their results with those of Nakamura (2009) and Imamura (2001), concluding that their model better matches the data given by Goto et al. (2010), even if the hypothesis of a landslide remains questionable. More recently, using an accurate seafloor topography and geological structure data, Okamura et al. (2018) suggested a new source, matching a collapse of the accretionary prism instead of active faults as suggested previously.

For the sake of simplicity and also because the aim of the present study is not to shed new light on the tsunami's origin, only the source

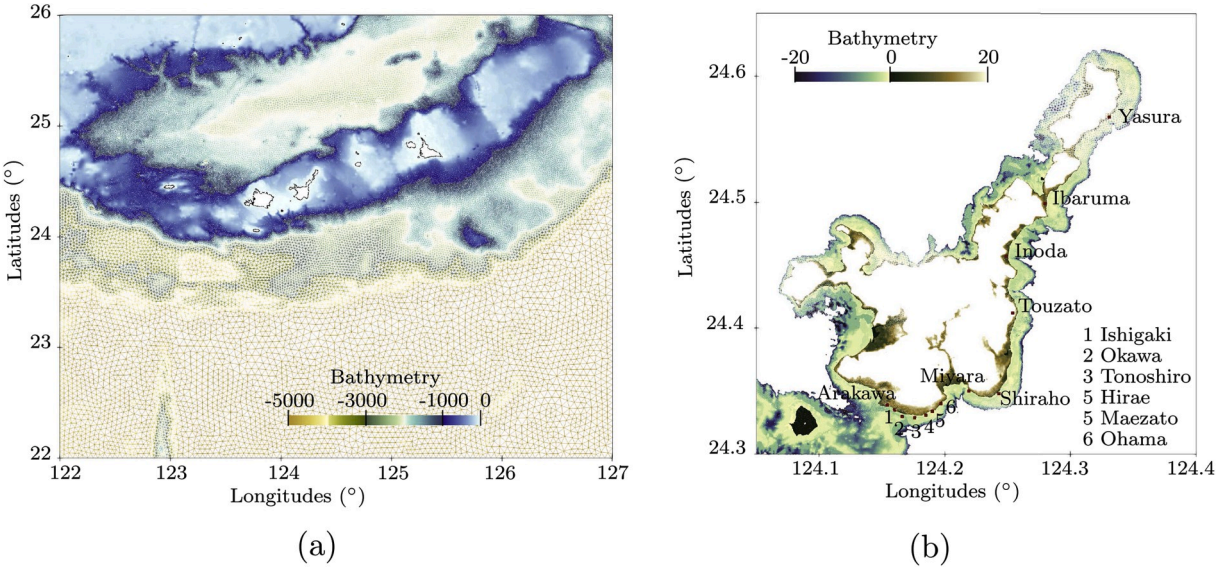

Fig. 3. Mesh generated for this study with the interpolated bathymetry and the reef. (3a) General view and complete mesh. (3b) A zoom around the Ishigaki Island with the reef representation and locations of the cities where run-up data are available. The black line is the model coastline.

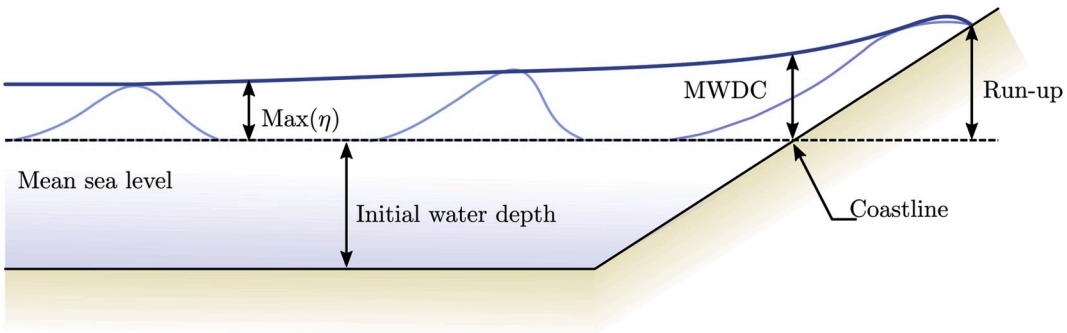

Fig. 4. Definition and sketch of tsunami run-up on a beach. η corresponds to the free surface elevation or wave height. MWDC indicates the Maximal Water Depth at the Coastline.

Table 1
Parameters of the tsunami source from Miyazawa et al. (2012).

	Lat.	Lon.	Length (km)	Width	Strike	Dip	Slip	Dislocation	Depth
	(◦)	(°)	(km)	(km)	(°)	(°)	(°)	(m)	(km)
Fault 1	24.2805	125.3722	70	35	240	70	90	12	5
Fault 2	23.9100	124.8000	72	36	259	70	90	12	5
Landslide	24.1348	124.2640	12	5	76	70	90	80	–

model from Miyazawa et al. (2012) have been considered. Fault characteristics are summarized in Table 1, representing the geometry and locations of different elements of the source.

From the above parameters, the method of Okada (1985) was applied to obtain the initial free surface of the propagation model. While applying the Okada method, the landslide is considered as an earthquake at the ground surface, as suggested by Miyazawa et al. (2012). The initial free surface condition of the model is presented in Fig. 5.

4. Numerical results

In this section, different versions of the numerical modelling of this event are presented. First, models with different friction coefficients were compared, allowing us to calibrate a reference model, Section 4.1. Then, using the calibrated model as reference, the RIF was estimated for a model without a reef, a model with the reef but without channels, and a model with a sea level change, Sections 4.2, 4.3 respectively.

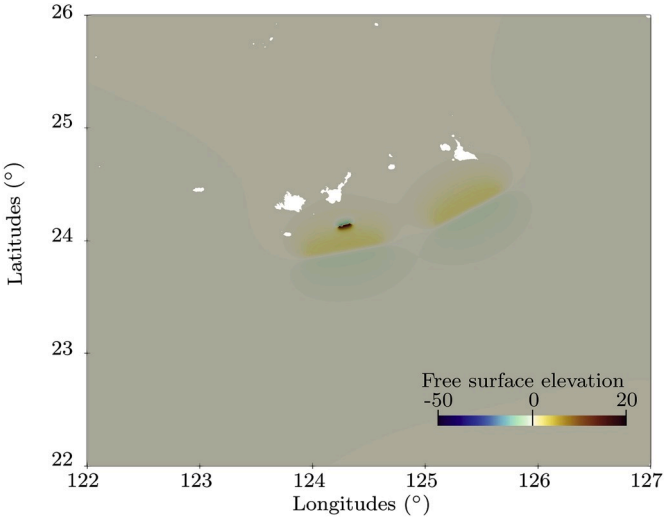

Fig. 5. Initial free surface elevation calculated using the Okada method (Okada, 1985) from the source parameters of Miyazawa et al. (2012).

4.1. Calibration of the model

The question about the bottom drag coefficient C_D and friction coefficient S in the reef has been raised many times (see Equation (2) for the relation between these two parameters).

In normal sea conditions, Rosman and Hench (2011) listed drag parameters C_D ranging from 0.015 to 0.8 for different kinds of reefs. From their *in situ* experiment at Ofu Island (American Samoa), Rogers et al. (2018) restricted this range to between 0.01 and 0.1, with an average around 0.03. For their characterization of the fringing reef at Ishigaki Island, Tamura et al. (2007) chose a slightly higher value of $C_D = 0.035$ for their drag coefficient.

In their model, Kunkel et al. (2006) used a drag coefficient from $C_D =$ 0.03 to 0.1, but noted that the value of drag coefficients of reefs are not well known. For tsunami studies, the friction coefficient independent of the water depth is usually used, see Equation (2). For the Samoa event, Gelfenbaum et al. (2011) used equivalent friction coefficients between $S = 10.4\ m^{1/3}.s^{-1}$ and $S = 50\ m^{1/3}.s^{-1}$, depending on the area. In the Philippines, Roeber and Bricker (2015) used a coefficient of $S \tilde{} 30\ m^{1/3}.s^{-1}$ and in a study of the Yaeyama tsunami, Miyazawa et al. (2012) used $S = 40\ m^{1/3}.s^{-1}$. In the reef area, the satellite-derived bathymetry grid gives an average depth of $h = 3.4\ m$, leading to $S \tilde{} 13.6\ m^{1/3}.s^{-1}$, if the drag coefficient is 0.035, as suggested by Tamura et al. (2007). However, considering the variability in measurements and estimates, plus the dependence on the health of the reef (Kunkel et al., 2006), few coefficient values have been tested to measure the influence of this choice and to calibrate the model to the data. Three values are tested: $S = 15, 20, 30\ m^{1/3}.s^{-1}$. Comparisons of run-ups obtained for these values of the Strickler coefficient are shown in Fig. 6 and compared to data from Goto et al. (2010).

The impact of the Strickler coefficient varies along the coastline due to the natural variation of the width and depth of the reef. As expected, the greatest stress ($S = 15\ m^{1/3}.s^{-1}$) gives the smallest run-ups, while the weakest stress ($S = 30\ m^{1/3}.s^{-1}$) gives higher estimates. Between the cities of Arakawa and Tonoshiro, the three simulations yield approximately the same range of values for run-ups, while differences between the models are larger for the highest run-ups (Ohama - Miyara - Shiraho). To better understand whether these differences are related to the interaction of waves with the reef or with shore topography after the coastline, wave signals in front of Ohama and Shiraho are compared

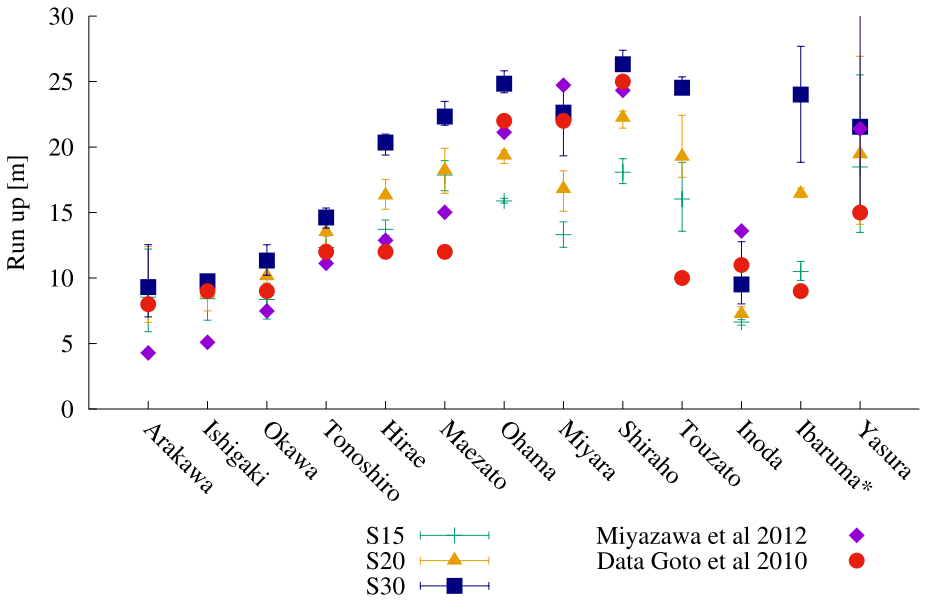

Fig. 6. Numerical run-ups for each Strickler coefficient model along the Ishigaki coastline. The location of the cities is shown on Map 3b. Run-ups are estimated at each location by considering at least 10 numerical points. The error bar represents the minimum, average and maximum values of the run-up at these points. The green tic, orange triangle, blue square correspond to $S = 15, 20, 30\, m^{1/3}/$ respectively. Red points indicate data from Goto et al. (2010) and purple diamonds are numerical results from Miyazawa et al. (2012). Ibaruma*, important error expected at Ibaruma, the run-up is estimated larger than 9 m by Goto et al. (2010), and around 30 m by Kawana (2000). (For interpretation of the references to color in this figure legend, the reader is referred to the Web version of this article.)

before and after the reef (Fig. 7). Time discretization does not allow an extremely fine description of the propagation of the wave. However, the wave signals match closely offshore, while differences in velocity and amplitude are observed at the shore. This comparison shows, as suggested by Gelfenbaum et al. (2011) and others, that representation of bottom friction in the reef area is essential, greatly affecting the results. Accordingly, it should be chosen carefully.

In Fig. 6, numerical results are compared to the numerical model from Miyazawa et al. (2012) (from whom the initialization model was taken). The differences obtained between our results and those of Miyazawa et al. could be due to the numerical grid and bathymetry, but also to the numerical model. Miyazawa et al. used a linear shallow water model for the open ocean while in the present study a nonlinear model was applied. The present model with $S = 30\ m^{1/3}.s^{-1}$ globally overestimates the data, but well represents the highest run-ups at Ohama, Miyara and Shiraho. Contrarily, models with $S = 15, 20\ m^{1/3}.s^{-1}$ do not represent the highest run-ups. For this reason, $S = 30\ m^{1/3}.s^{-1}$ was considered valid to represent hydrodynamic processes during this event, and it was employed for the rest of this study. It corresponds to a smaller drag stress than that suggested by Tamura et al. (2007).

4.2. The model without a reef

To measure the impact of reef structure on the south and east coasts, a numerical model without a reef was built and compared to the original with-reef model. The bottom in the reef area was smoothed using a filter function of Telemac2D on the bathymetry data grid. This filter corresponds to mass-lumping smoothing, using the mass matrix generated for the Finite Element method. The filter was applied 100 times to obtain a bottom without a reef. A comparison of the bathymetry with and without a reef is shown in Fig. 8.

The RIF, defined in Paragraph 2.3 was calculated between the modified reef model (without a reef) and the reference model (with a reef). It is plotted along the coastlines in Fig. 9.

The RIF fluctuates considerably along the coastline. However, for most regions, it remains positive, meaning that the absence of the reef led to an amplification of the wave. At some locations, the RIF decreases to negative values. Nearly always these locations correspond to a channel in the reef (Fig. 9).

To estimate how much reef channels impact the results, a second numerical model with a full reef was developed. In this model, the bathymetry corresponds to the original reef bathymetry in which the channels identified in Fig. 9, were artificially filled. A new RIF was calculated for this full reef model (Fig. 9). As expected, along almost the entire length of the coastline, the RIF remains null. However, near areas where channels are supposed to be, the RIF decreases drastically. It is clear that channels amplify tsunami waves (further discussed below). Moreover, at these locations, the RIF of the full reef model is smaller than the RIF of the model without reef, suggesting that a channel in a reef induces a larger inundation of the nearby coast than with no reef at all.

4.3. Initial sea level effect on the coastline wave heights

Due to different physical phenomena, such as tidal or sea level rises from climate change, the initial sea level can vary. As suggested in Kunkel et al. (2006), Gelfenbaum et al. (2011), Shao et al. (2019), this change should not drastically impact the propagation of the wave offshore, but may impact the propagation of the wave in the coastal zone and at the shore. Indeed, the initial sea level regulates reef depth, thereby influencing interactions between the reef and waves. To investigate this parameter, we modified the bathymetry of the model by decreasing or increasing the bottom elevation. Four new sea levels were tested, corresponding to different states of the tide. From Goto et al. (2010), the tidal range is 2 m at Ishigaki Island. The new sea levels corresponded to the high tide ($+$ 1 m), mid-high tide ($+$ 0.5 m), mid-low tide ($-$ 0.5 m) and low tide ($-$ 1 m). As performed for the model without the reef, the results obtained with a tide level change were compared to the original model (Fig. 10) by calculating a new RIF from the modified reef depth models.

As for the model without the reef, the RIF varies along the coastline. However, a general trend can be identified. The MWDC increases with reef depth. Lower tides result in smaller waves at the coastline, whereas higher tides produce larger waves.

At some locations, this trend does not apply, and either the tide models converge, or else the high tide model yields a smaller MWDC than the low tide model. Again these locations appear to be situated close to reef channels identified in Fig. 9.

5. Discussion and conclusions

The aim of this study was to determine the impact of the reef along the south and east coasts of Ishigaki Island on the inundation that occurred during the 1771 Yaeyama tsunami, following the method used

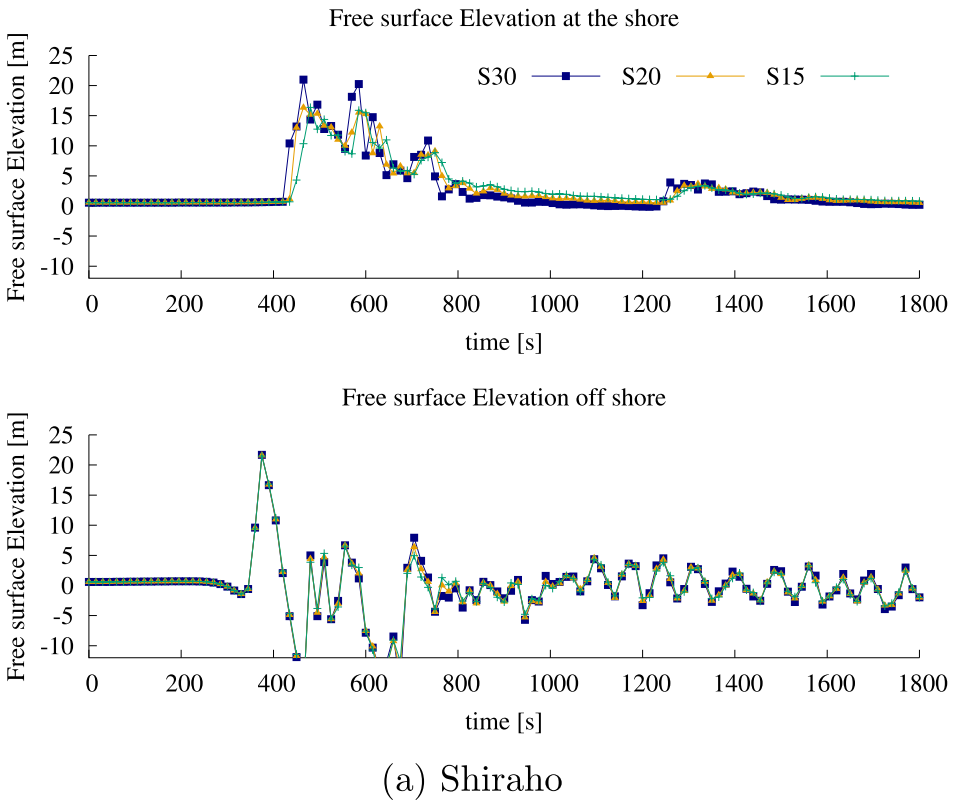

(a) Shiraho

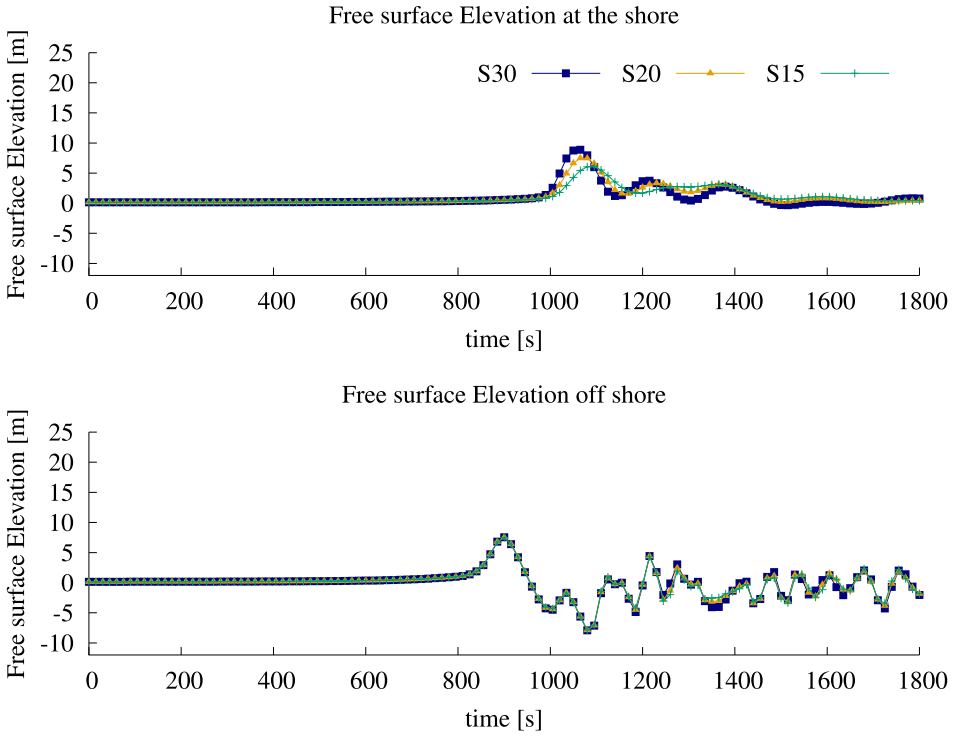

(b) Yasura

Fig. 7. Temporal evolution of the free surface elevation at Shiraho and Yasura before the reef (Off shore) and at the coastline (shore) for the Strickler coefficient $S = 15, 20, 30\ m^{1/3}.s^{-1}$.

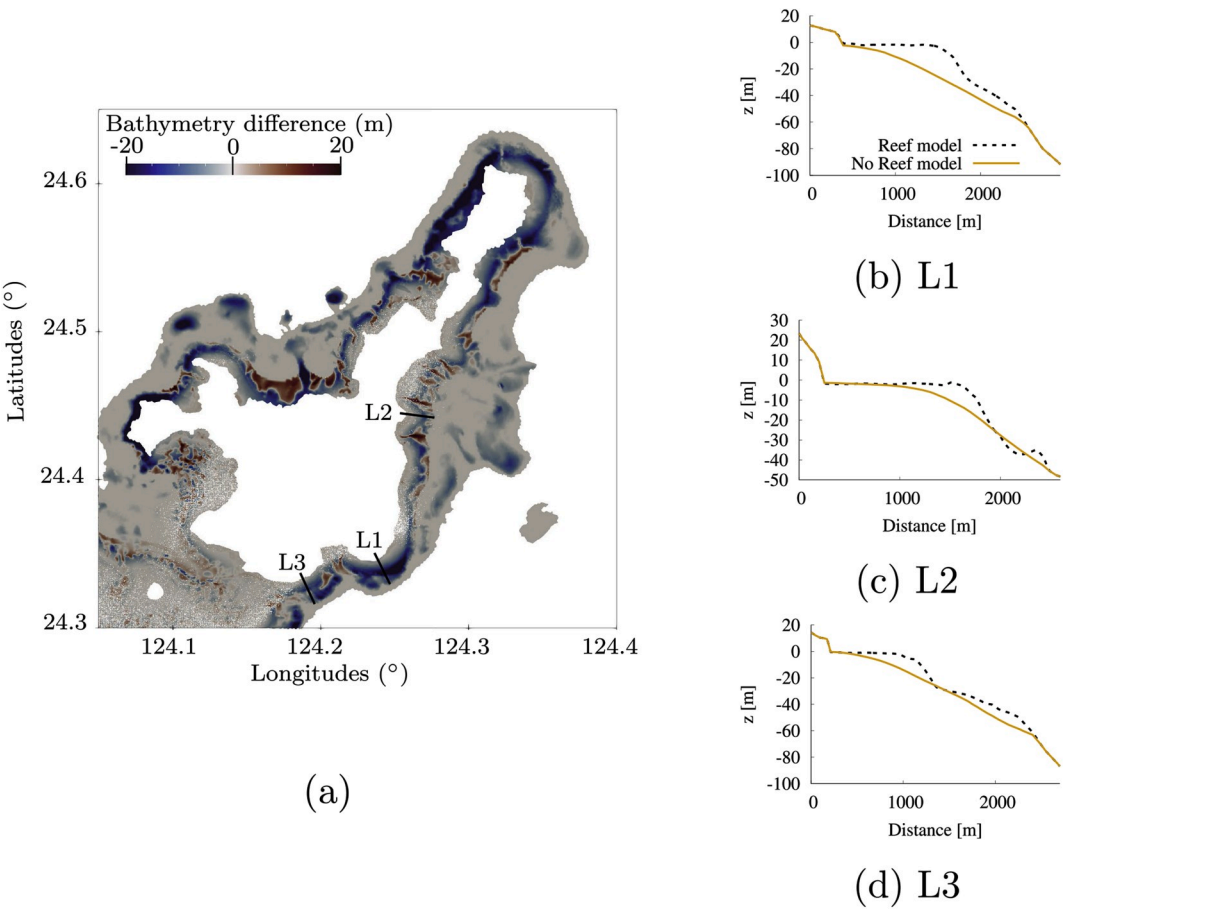

Fig. 8. Comparison of bathymetry between the model with and without a reef after performing the smoothing process. (8a) Maps of the difference in meters between the model with and without reef bathymetry. L1, L2, L3 represent the cross-sections shown in graphs (8b), (8c), (8d) respectively. The dashed black line represents bathymetry with the reef. The orange plain line is the bathymetry without the reef. (For interpretation of the references to color in this figure legend, the reader is referred to the Web version of this article.)

by Baba et al. (2008) on the Great Barrier reef in Australia.

Our results agree with previous experimental work and numerical models created for other locations. Calibration of our model confirms that roughness is an important parameter, as noted by Dilmen et al. (2018) and Gelfenbaum et al. (2011), among others. As shown in Fig. 6, inundation and run-up elevations are not uniformly impacted by changes in the Strickler coefficient. Bifurcations between models occur during the propagation of waves over reefs, illustrating the importance of the representation of frictional stress in these areas (Fig. 7). For a Strickler coefficient varying from 15 to 30 $m^{1/3}.s^{-1}$, the estimated run-up varies from 10 m to 25 m at Ibaruma (Fig. 6), whereas at other locations, the range is less (only 3 m at Ishigaki city). This suggests that the common use of a uniform bottom friction representation (as used in this study) is not necessarily valid for specific reef cases, as also demonstrated previously (Gelfenbaum et al., 2011). From comparisons with run-up data (Goto et al., 2010), the frictional coefficient was set to $S = 30\ m^{1/3}.s^{-1}$, which allows representation of larger run-ups, even if it over-estimates inundation at other locations.

To compare models with and without a reef, so as to measure the effect of the reef, a new parameter, the Reef Impact Factor was defined (see Equation (3)). Looking at evolution of the RIF (Fig. 9), a general increasing trend between 10% and 20% (12.5% on average) is observed along the coast without the reef, with a maximum of 160% at the extreme north end. This suggests that most of the coast is protected by the reef. However, in some areas, the absence of a reef caused a decreased RIF, thus a smaller maximum water depth at the coast (MWDC).

Almost all these locations face gaps or channels in the reef. This shows the importance of their role as investigated theoretically by Kunkel et al. (2006); Gelfenbaum et al. (2011); Roger et al. (2014) and highlighted by Fernando et al. (2005) in Sri Lanka for the 2004 Sumatra tsunami. By artificially filling these gaps, and creating a full reef model, the MWDC in front of these gaps is reduced up to 40% south of Inoda (see evolution of the RIF, Fig. 9). This increase in flooding due to channels is drastically more important than the 9% predicted by Gelfenbaum et al. (2011). However, channel width impacts its influence (Roger et al., 2014), and the present channels are wider ($500 - 1500\ m$) than those considered by Gelfenbaum et al. (2011) (100 m). The full reef model yields a smaller RIF than the model without the reef in the zone facing the gap, suggesting that for the adjacent coast, reef channels are more harmful than no reef at all. More than reducing the reef protection effectiveness, channels enhance inundation by focusing tsunami wave energy. This same conclusion was drawn by Nott (1997), where entrances in the Great Reef Barrier may have enhanced and amplified paleotsunamis; and by Gelfenbaum et al. (2011) for embayments and embayment-channel combinations, where the relative increase of inundation was estimated at 25% and 55%, respectively. The difference between embayments and channels relates to their depth, as embayments are above sea level while channels are entirely immersed. Similarly, Leuven et al. (2019) suggested this behaviour for estuaries during sea-level-rise-plus-tidal flooding, enhancing the importance of estuary width. In light of this similarity, the shape of a channel may have a greater impact than its depth, since channels seem to act like embayments.

In addition, channels impact a wide portion of the coast. For

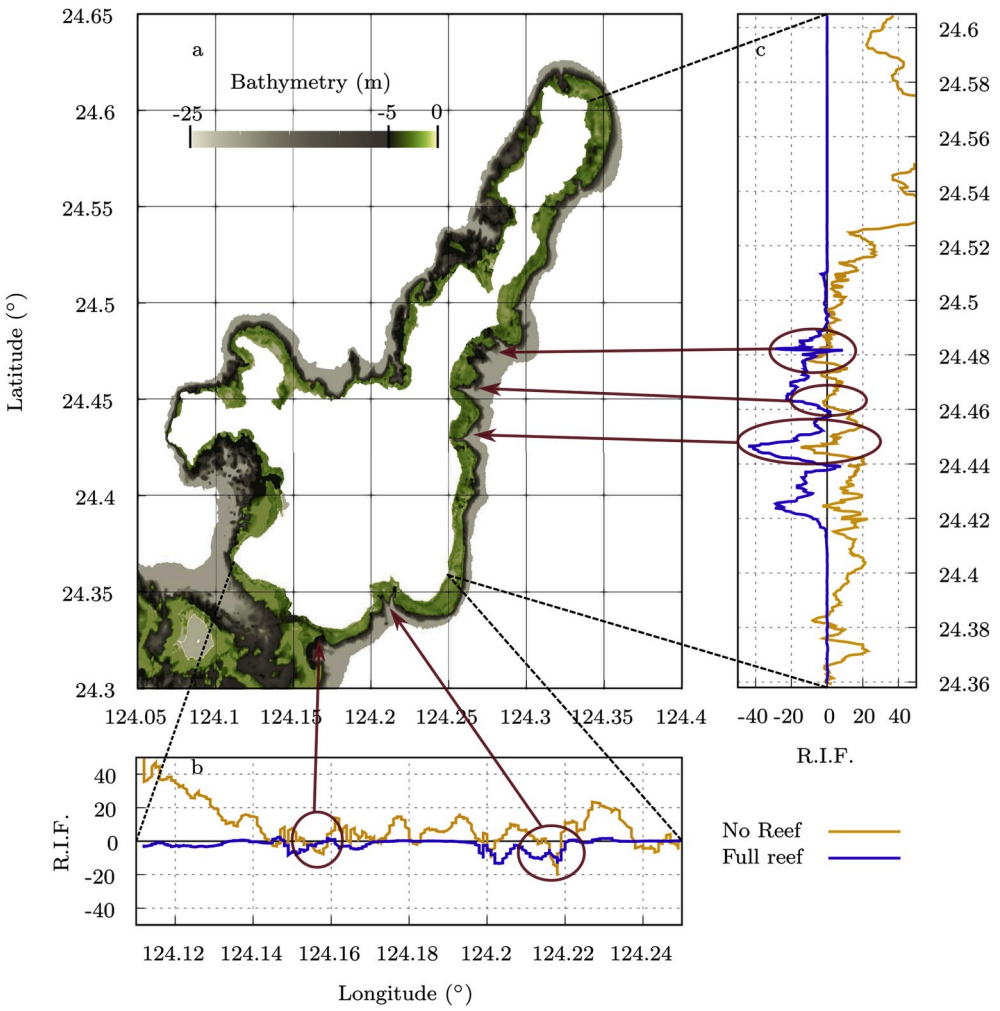

Fig. 9. (a) Map of numerical reef bathymetry of Ishigaki Island used for the original reef model. (b) Evolution of the Reef Impact Factor (RIF) along the southern coast. Orange and blue lines correspond to the RIF (see Equation (3)) for the no-reef model and the model with the channel artificially filled (full reef), respectively. For sake of clarity, the RIF curves are smoothed every 10 points along the coast. (c) same as (b) but on the east coast. Arrows and circles point to zones along the coast where the RIF is negative. (For interpretation of the references to color in this figure legend, the reader is referred to the Web version of this article.)

example, approximately 4.4 km of the coast, between Inoda and Touzato (from latitude 24.42° to 24.45° on Fig. 9) was affected by a channel 1.5 km wide at its mouth. This effect was also highlighted by Kunkel et al. (2006) where around 8% of the circular island coast was affected by a gap in its reef due to diffraction of the waves; and by Roger et al. (2014) who emphasized that waves passing through the gap could lead to resonance or refractive effects between the shoreline and the reef. Moreover, the absence of the 180-m-wide channel, following the Ishigaki city coast, slightly decreases the highest waves along the south coast (by up to 5% on average), suggesting that this channel distributed the tsunami energy along 6 km of shoreline. As highlighted by Gelfenbaum et al. (2011) and illustrated by the diversity of previous conclusions, the effect of reef gaps is still poorly understood.

Kunkel et al. (2006), among others, identified reef depth as one of the key reef parameters influencing inundation. This parameter naturally varies with the tide. Following the method of Gelfenbaum et al. (2011), the sea level was varied in this study to examine how reef impact varies depending on this parameter (Fig. 10). In general, the MWDC and the resulting RIF at the coast increase with initial water depth over the reef, as the friction stress decreases with increasing depth. This conclusion agrees with the studies of Gelfenbaum et al. (2011) and Shao et al. (2019). Both of these one-dimensional studies observed increased inundation distance with tide and with sea level rise, respectively. In the present study, this increase is not uniform along the shore. Along the southwestern coast, the MWDC varies ± 40%, depending on the tide, but on average, it stays within 10%. This value shows a weak dependence on reef depth compared to channel effects. This behaviour has also been observed by Roger et al. (2014) who claimed that the impact of reef width surpassed that of reef depth.

In front of reef channels, the above trend does not apply. Instead the tide does not seem to impact the MWDC and sometimes even decreases during high tide. Aside from the impact of channels, a few other locations present an inverse trend, with slightly larger MWDC during low tide than high tide, such as at longitude 124.235° along the south coast or between the latitudes 24.38° and 24.40° on the east coast, for instance. This kind of scenario is absent in the studies of Shao et al. (2019) and Gelfenbaum et al. (2011), suggesting a 2D resonance or refraction effect in these cases. Resonant waves have been highlighted by Péquignet et al. (2009); Pearson et al. (2017) and estimated by Gawehn et al. (2016) to occur 3.5% of the time during regular wave-driven flooding. Roeber et al. (2010) analyzed different resonance modes of the 2009 Samoa tsunami at Tutulia island due to the 2D geomorphology of the island and its embayments, noting that shallow reefs could amplify tsunamis, and explaining the discrepancy in the run-up observations along the shore for this event.

On the northern coast (latitudes > 24.52°), the impact of the initial sea level, as well as the impact of the reef presence is more pronounced than along other parts of the coast. This section of the coast is furthest from the source and the main waves of the event. As a consequence, wave parameters are very different. The maximal free surface along the reef edge ($z = -10\ m$) varies from less than 10 m to more than 25 m (see Fig. 11a) and the wave period changes from around 242 s in front of Yasura to 110 s in front of Shiraho (see Fig. 11b).

While the reef width and depth are more or less homogeneous in

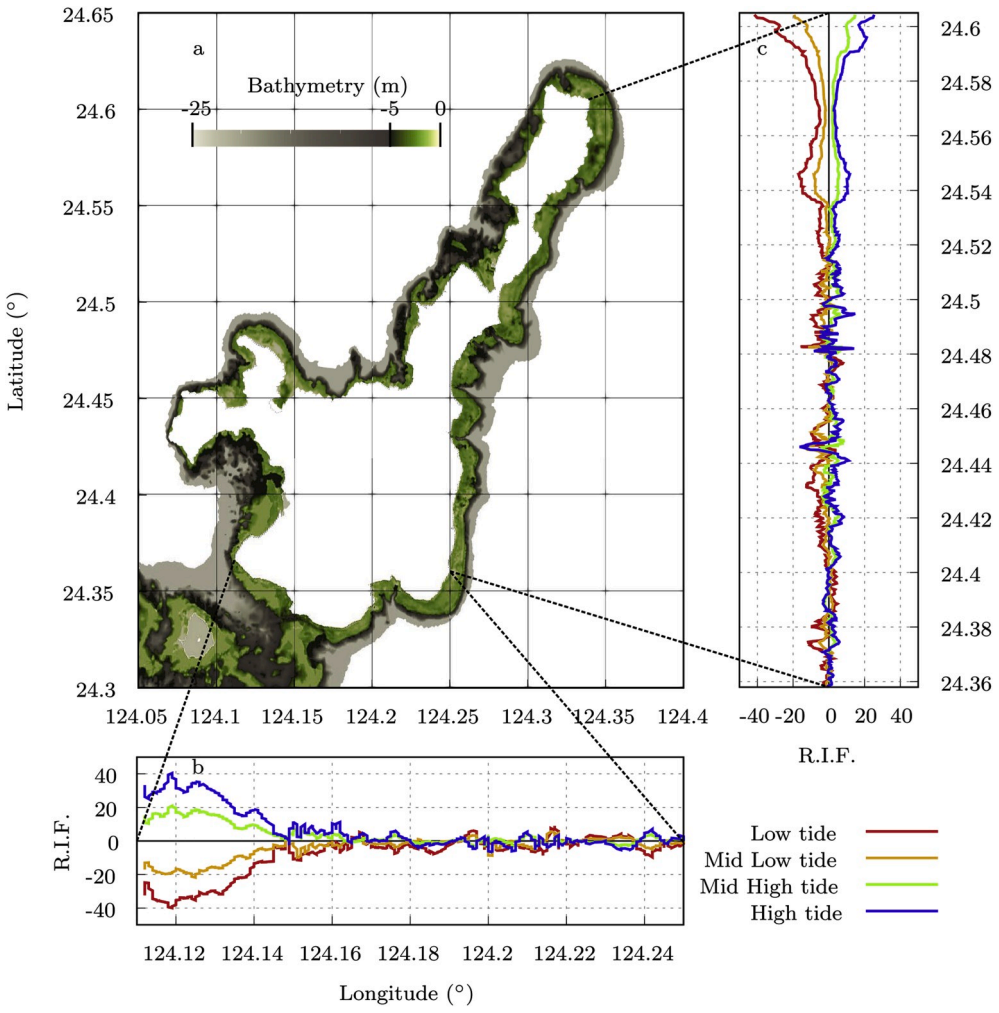

Fig. 10. Same as Fig. 9 but for the high, mid-high, mid-low, low tide models.

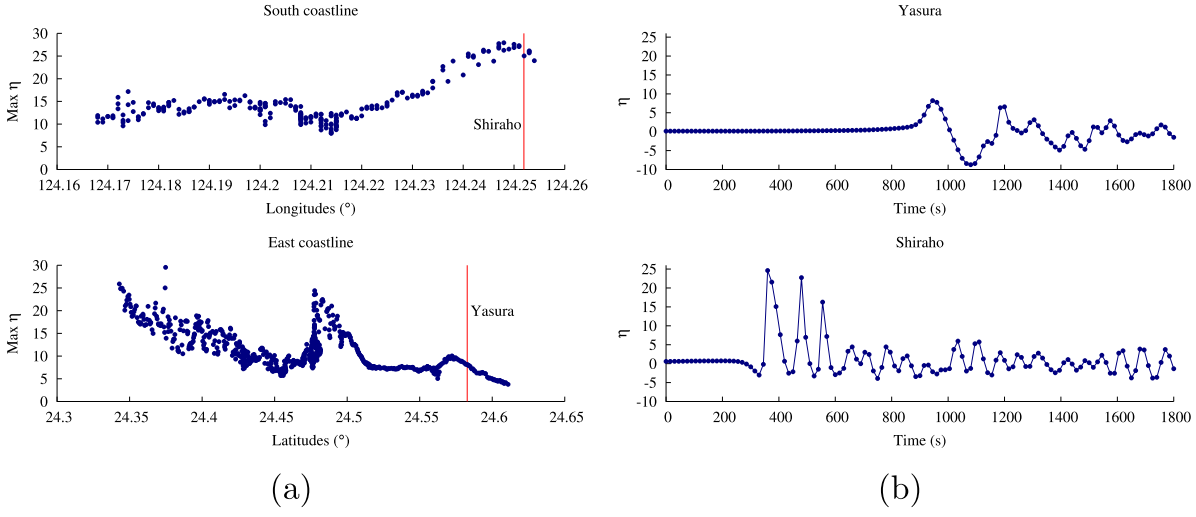

Fig. 11. Wave parameters of the Meiwa tsunami event. (11a) Temporal maximal free surface elevation η of the incident waves at the edge of the reef ($z = -10\,m$) along the South and East coastlines, top and bottom graphs respectively. Red lines mark the location of Shiraho and Yasura areas. (11b) Evolution of the free surface elevation at the reef edge ($z = -10\,m$) in front of Yasura and Shiraho, top and bottom respectively. (For interpretation of the references to color in this figure legend, the reader is referred to the Web version of this article.)

these two areas, this change of wave amplitude and period may influence reef interactions. In the present study, the RIF was smaller for the steepest wave (Shiraho 's wave); thus, reef protection was reduced. This statement is consistent with Kunkel et al. (2006) and Lynett (2007), in which an increase of wave steepness led to decreased reef and obstacle effectiveness. Thus, a change in reef parameters, such as initial reef depth, may have a greater influence for less steep waves, as observed along the northern coast, in front of Yasura.

Similarly, reefs have a greater impact on inundation in the western part of the South coast. Unlike the northern coast, this part of the coast does not receive direct incident waves. Only incident waves propagating over a larger reef area or through the narrow channel following the coast from the East reach this coast. As shown by Kunkel et al. (2006) and Gelfenbaum et al. (2011), wider reefs have stronger effects, as friction process supercedes the shoaling mechanism. Moreover, Gelfenbaum et al. (2011) showed that the impact of the tide increases with reef width. Thus, the higher RIF value along this part of the coast can be explained by these two conclusions.

On average, the RIF is around 12.5%, suggesting a smaller impact of the reef than the 80% reduction estimated by Ferrario et al. (2014) for regular or non-tsunami wave driven flooding. For regular situations, reef width, slope and bed friction have been identified as key parameters (Gourlay, 1994; Quataert et al., 2015; Tajima et al., 2016; Pearson et al., 2017), with particular emphasis on reef depth (Péquignet et al., 2011), justifying the common concern about sea level rise due to climate change (Beetham et al., 2017; Storlazzi, 2018; Pearson et al., 2017). However, in the present study, except in the two areas described above, reef depth does not seem to drastically influence the impact of the reef on tsunami inundation. These differences, regarding the effectiveness of reefs as barriers and the impact of reef depth, between regular and the present tsunami flooding, suggest that incident wave parameters are more important than previously realized.

The present study confirms that the complexity of the interaction between reefs and tsunamis prevents generalized or universal approaches to the problem, and that tsunami flooding should be considered different than regular flooding. As already mentioned by Baba et al. (2008), each reef and associated events require dedicated study accounting for local bathymetry, the reef friction parameter, the existence of channels, and the wave signal. However, in order to further advance our understanding, a deeper study of reef structure at different locations along the coast may allow grouping and identification of specific reef morphologies, as performed by Costa et al. (2016) for the Brazilian coast. This kind of analysis will allow identification of the main parameters with real 2D bathymetry, and could address the question of reef slope, which was not investigated in the present study. Using this with the RIF will allow us to link these main parameters to the impact of the reef on the inundation.

Reefs are not considered in early tsunami warning (Kamigaichi, 2009). It is therefore important to assess their impact beforehand, and to take them into account during the creation of inundation maps or potential hazard map together with the RIF. Indeed, the RIF corresponds to a process-based indicator as defined by Ferreira et al. (2017) for sandy coasts. To go further, the RIF is a straight forward indicator of the consequences of modifications in the reef structure that coastal managers can consider, such as when digging or widening a channel or a pit (Klaver et al., 2019).

In conclusion, this study contributes to the global effort to better understand reef-tsunami interactions, with a particular emphasis on the contribution of reef channels and reef depth. Moreover, a new indicator, the RIF has been defined, allowing us to quantify and clearly determine the influence of reefs along coastlines without taking shore topography into account, allowing consistent comparisons between different idealized and non-idealized reefs. In the case of the 1771 tsunami event, the south-east reef of Ishigaki protected the coast, by about 12.5% on average. However, channels and gaps in reefs lead to significant amplification of inundation along the adjacent coast, revealing vulnerable areas. Following the report by Fernando et al. (2005), these consequences support concerns about reef protection.

Declaration of competing interest

The authors declare that they have no known competing financial interests or personal relationships that could have appeared to influence the work reported in this paper.

Acknowledgments

The authors thank Kazumi Inoha from the Marine Biophysics Unit for her work in generating the satellite-derived bathymetry grid, and the Scientific Computing and Data Analysis Section at OIST for its support. The authors also thank Dr. Riadh Ata for his feedback and advice on the project.

References

Araoka, D., Yokoyama, Y., Suzuki, A., Goto, K., Miyagi, K., Miyazawa, K., Matsuzaki, H., Kawahata, H., Aug. 2013. Tsunami recurrence revealed by Porites coral boulders in the southern Ryukyu Islands, Japan. Geology 41 (8), 919–922.

Baba, T., Mleczko, R., Burbidge, D., Cummins, P.R., Thio, H.K., 2008. The effect of the Great barrier reef on the propagation of the 2007 Solomon Islands tsunami recorded in Northeastern Australia. In: Cummins, P.R., Satake, K., Kong, L.S.L. (Eds.), Tsunami Science Four Years after the 2004 Indian Ocean Tsunami. Birkhäuser Basel, Basel, pp. 2003–2018.

Baird, A.H., Campbell, S.J., Anggoro, A.W., Ardiwijaya, R.L., Fadli, N., Herdiana, Y., Kartawijaya, T., Mahyiddin, D., Mukminin, A., Pardede, S.T., Pratchett, M.S., Rudi, E., Siregar, A.M., Nov. 2005. Acehnese reefs in the wake of the Asian tsunami. Curr. Biol. 15 (21), 1926–1930.

Becker, J.J., Sandwell, D.T., Smith, W.H.F., Braud, J., Binder, B., Depner, J., Fabre, D., Factor, J., Ingalls, S., Kim, S.-H., Ladner, R., Marks, K., Nelson, S., Pharaoh, A., Trimmer, R., Von Rosenberg, J., Wallace, G., Weatherall, P., Nov. 2009. Global bathymetry and elevation data at 30 arc seconds resolution: SRTM30_PLUS. Mar. Geodes. 32 (4), 355–371.

Beetham, E., Kench, P.S., Popinet, S., Oct. 2017. Future reef growth can mitigate physical impacts of sea-level rise on Atoll islands: sea-level rise impacts on atoll islands. Earth's Future 5 (10), 1002–1014.

Costa, M.B., Araújo, M., Araújo, T.C., Siegle, E., 2016. Influence of reef geometry on wave attenuation on a Brazilian coral reef. Geomorphology 253, 318–327.

Dilmen, D.I., Roe, G.H., Wei, Y., Titov, V.V., Apr. 2018. The role of near-shore bathymetry during tsunami inundation in a reef island setting: a case study of Tutuila island. Pure Appl. Geophys. 175 (4), 1239–1256.

Fernando, H.J.S., McCulley, J.L., Mendis, S.G., Perera, K., 2005. Coral poaching worsens tsunami destruction in Sri Lanka. Eos Trans. AGU 86 (33), 301.

Ferrario, F., Beck, M.W., Storlazzi, C.D., Micheli, F., Shepard, C.C., Airoldi, L., Sep. 2014. The effectiveness of coral reefs for coastal hazard risk reduction and adaptation. Nat. Commun. 5 (1), 3794.

Ferreira, Ó., Plomaritis, T.A., Costas, S., Oct. 2017. Process-based indicators to assess storm induced coastal hazards. Earth Sci. Rev. 173, 159–167.

Gawehn, M., van Dongeren, A., van Rooijen, A., Storlazzi, C.D., Cheriton, O.M., Reniers, A., Oct. 2016. Identification and classification of very low frequency waves on a coral reef flat: classification of VLF waves. J. Geophys. Res. Oceans 121 (10), 7560–7574.

Gelfenbaum, G., Apotsos, A., Stevens, A.W., Jaffe, B., Jul. 2011. Effects of fringing reefs on tsunami inundation: American Samoa. Earth Sci. Rev. 107 (1–2), 12–22.

Goto, K., Kawana, T., Imamura, F., Sep. 2010. Historical and geological evidence of boulders deposited by tsunamis, southern Ryukyu Islands, Japan. Earth Sci. Rev. 102 (1–2), 77–99.

Gourlay, M., May 1994. Wave transformation on a coral reef. Coast. Eng. 23 (1–2), 17–42.

Grilli, S.T., Grilli, A.R., David, E., Coulet, C., Jun. 2016. Tsunami hazard assessment along the north shore of Hispaniola from far- and near-field Atlantic sources. Nat. Hazards 82 (2), 777–810.

Hervouet, J.-M., 2007. Hydrodynamics of Free Surface Flows: Modelling with the Finite Element Method, vol. 360. Wiley Online Library.

Hongo, C., Kawamata, H., Goto, K., Jun. 2012. Catastrophic impact of typhoon waves on coral communities in the Ryukyu Islands under global warming: catastrophic impact of typhoon on corals. J. Geophys. Res. 117 (G2) (n/a–n/a).

Horsburgh, K.J., Wilson, C., Baptie, B.J., Cooper, A., Cresswell, D., Musson, R.M.W., Ottemöller, L., Richardson, S., Sargeant, S.L., Apr. 2008. Impact of a Lisbon-type tsunami on the U.K. coastline and the implications for tsunami propagation over broad continental shelves. J. Geophys. Res. 113 (C4), C04007.

Imamura, F., 2001. Numerical study of the 1771 Meiwa tsunami at Ishigaki Island, Okinawa and the movement of the tsunami stones. In: Proceedings of Coastal Engineering, vol. 48. JSCE, pp. 346–350.

Jarvis, A., Guevara, E., Reuter, H.I., Nelson, A.D., 2008. Hole-filled SRTM for the globe: Version 4: Data grid.

JHA, 2016. Bathymetrymapper. Japan hydrographic association. in Japanese. http://fields.canpan.info/report/detail/19931.
JHA, RESTEC, JCG, 2016. Survey and Research of Grasping Shallow Water Depth Information Using Satellite Imagery in 2016. Nippon Foundation Japan Foundation.
Kamigaichi, O., 2009. Tsunami forecasting and warning. In: Meyers, R.A. (Ed.), Encyclopedia of Complexity and Systems Science. Springer New York, New York, NY, pp. 9592–9618.
Kawana, T., 2000. Field Guidebook for Tsunami Disaster Prevention. Research Association for Tokai, To-Nankai and Nankai Earthquake Tsunamis. Osaka 25.
Klaver, S., Nederhoff, C.M., Giardino, A., Tissier, M.F.S., Dongeren, A.R., Spek, A.J.F., Apr. 2019. Impact of coral reef mining pits on nearshore hydrodynamics and wave runup during extreme wave events. J. Geophys. Res. Oceans 124 (4), 2824–2841.
Kunkel, C.M., Hallberg, R.W., Oppenheimer, M., Dec. 2006. Coral reefs reduce tsunami impact in model simulations. Geophys. Res. Lett. 33 (23), L23612.
Le Gal, M., Violeau, D., Ata, R., Wang, X., Sep. 2018. Shallow water numerical models for the 1947 gisborne and 2011 Tohoku-Oki tsunamis with kinematic seismic generation. Coast. Eng. 139, 1–15.
Leuven, J.R.F.W., Pierik, H.J., van der Vegt, M., Bouma, T.J., Kleinhans, M.G., Dec. 2019. Sea-level-rise-induced threats depend on the size of tide-influenced estuaries worldwide. Nat. Clim. Change 9 (12), 986–992.
Liu, P.-F., 2009. Tsunami. In: Encyclopedia of Ocean Sciences. Elsevier, pp. 127–140.
Lynett, P.J., Nov. 2007. Effect of a shallow water obstruction on long wave runup and overland flow velocity. J. Waterw. Port, Coast. Ocean Eng. 133 (6), 455–462.
Lyzenga, D., Malinas, N., Tanis, F., Aug. 2006. Multispectral bathymetry using a simple physically based algorithm. IEEE Trans. Geosci. Rem. Sens. 44 (8), 2251–2259.
Miyazawa, K., Goto, K., Imamura, F., 2012. Re-evaluation of the 1771 Meiwa tsunami source model, southern Ryukyu islands, Japan. In: Submarine Mass Movements and Their Consequences. Springer, pp. 497–506.
Nakamura, M., Oct. 2009. Fault model of the 1771 Yaeyama earthquake along the Ryukyu Trench estimated from the devastating tsunami. Geophys. Res. Lett. 36 (19), L19307.
Nakata, T., Kawana, T., 1995. Historical and prehistorical large tsunamis in the southern Ryukyus, Japan. In: El-Sabh, M.I., Tsuchiya, Y., Shuto, N. (Eds.), Tsunami: Progress in Prediction, Disaster Prevention and Warning, vol. 4. Springer Netherlands, Dordrecht, pp. 211–221.
Nott, J., Sep. 1997. Extremely high-energy wave deposits inside the Great Barrier Reef, Australia: determining the cause—tsunami or tropical cyclone. Mar. Geol. 141 (1–4), 193–207.
NRC, 2010. Blue Kenue™: Software Tool for Hydraulic Modellers.
Okada, Y., 1985. Surface deformation due to shear and tensile faults in a half-space. Bull. Seismol. Soc. Am. 75 (4), 1135–1154.
Okamura, Y., Nishizawa, A., Fujii, Y., Yanagisawa, H., 2018. Accretionary prism collapse: a new hypothesis on the source of the 1771 giant tsunami in the Ryukyu Arc, SW Japan. Sci. Rep. 8 (1), 13620.
Opentelemac, Accessed 8 April 2020. opentelemac.org.
Pearson, S.G., Storlazzi, C.D., van Dongeren, A.R., Tissier, M.F.S., Reniers, A.J.H.M., Dec. 2017. A Bayesian-based system to assess wave-driven flooding hazards on coral reef-lined coasts. J. Geophys. Res. Oceans 122 (12), 10099–10117.
Péquignet, A.-C., Becker, J.M., Merrifield, M.A., Boc, S.J., Jun. 2011. The dissipation of wind wave energy across a fringing reef at Ipan, Guam. Coral Reefs 30 (S1), 71–82.
Péquignet, A.C.N., Becker, J.M., Merrifield, M.A., Aucan, J., Feb. 2009. Forcing of resonant modes on a fringing reef during tropical storm Man-Yi: forcing of resonant modes on a reef. Geophys. Res. Lett. 36 (3) (n/a–n/a).
Quataert, E., Storlazzi, C., van Rooijen, A., Cheriton, O., van Dongeren, A., Aug. 2015. The influence of coral reefs and climate change on wave-driven flooding of tropical coastlines: influence of coral reefs on flooding. Geophys. Res. Lett. 42 (15), 6407–6415.
Roeber, V., Bricker, J.D., Nov. 2015. Destructive tsunami-like wave generated by surf beat over a coral reef during Typhoon Haiyan. Nat. Commun. 6 (1), 7854.
Roeber, V., Yamazaki, Y., Cheung, K.F., Nov. 2010. Resonance and impact of the 2009 Samoa tsunami around Tutuila, American Samoa: resonance and impact of 2009 Samoa tsunami. Geophys. Res. Lett. 37 (21) (n/a–n/a).
Roger, J., Dudon, B., Krien, Y., Zahibo, N., 2014. Discussion about tsunami interaction with fringing coral reef. In: Tsunami Events and Lessons Learned. Springer, pp. 161–176.
Rogers, J.S., Maticka, S.A., Chirayath, V., Woodson, C.B., Alonso, J.J., Monismith, S.G., Jul. 2018. Connecting flow over complex Terrain to hydrodynamic roughness on a coral reef. J. Phys. Oceanogr. 48 (7), 1567–1587.
Rosman, J.H., Hench, J.L., Aug. 2011. A framework for understanding drag parameterizations for coral reefs. J. Geophys. Res. 116 (C8), C08025.
Roy, D., Wulder, M., Loveland, T., C.E.,W., Allen, R., Anderson, M., Helder, D., Irons, J., Johnson, D., Kennedy, R., Scambos, T., Schaaf, C., Schott, J., Sheng, Y., Vermote, E., Belward, A., Bindschadler, R., Cohen, W., Gao, F., Hipple, J., Hostert, P., Huntington, J., Justice, C., Kilic, A., Kovalskyy, V., Lee, Z., Lymburner, L., Masek, J., McCorkel, J., Shuai, Y., Trezza, R., Vogelmann, J., Wynne, R., Zhu, Z., Apr, 2014. Landsat-8: science and product vision for terrestrial global change research. Rem. Sens. Environ. 145, 154–172.
Shao, K., Liu, W., Gao, Y., Ning, Y., Jan. 2019. The influence of climate change on tsunami-like solitary wave inundation over fringing reefs. J. Integr. Environ. Sci. 16 (1), 71–88.
Storlazzi, C., May 2018. Challenges of forecasting flooding on coral reef–lined coasts. Eos 99.
Strickler, A., 1981. Contributions to the Question of a Velocity Formula and Roughness Data for Streams, Channels and Closed Pipelines.
Suzuki, R., 2005. Characteristics of Bioerosion by Echinometra mathaei on the fringing reef of the Ishigaki island, the Ryukyus, Japan. 地域学研究 (18), 1–39.
Synolakis, C.E., 1991. Tsunami runup on steep slopes: how good linear theory really is. In: Bernard, E.N. (Ed.), Tsunami Hazard. Springer Netherlands, Dordrecht, pp. 221–234.
Tajima, Y., Shimozono, T., Gunasekara, K.H., Cruz, E.C., Mar. 2016. Study on locally varying inundation characteristics induced by super typhoon Haiyan. Part 2: deformation of storm waves on the beach with fringing reef along the east coast of eastern samar. Coast Eng. J. 58 (1), 1640003–1–1640003–24.
Tamura, H., Nadaoka, K., Paringit, E.C., Mar. 2007. Hydrodynamic characteristics of a fringing coral reef on the east coast of Ishigaki Island, southwest Japan. Coral Reefs 26 (1), 17–34.
Violeau, D., Ata, R., Benoit, M., Joly, A., Abadie, S., Clous, L., Medina, M.M., Morichon, D., Chicheportiche, J., Le Gal, M., 2016. A database of validation cases for tsunami numerical modelling. In: Sustainable Hydraulics in the Era of Global Change: Proceedings of the 4th IAHR Europe Congress (Liege, Belgium, 27-29 July 2016). CRC Press, p. 377.
Weiss, R., Feb. 2012. The mystery of boulders moved by tsunamis and storms. Mar. Geol. 295–298, 28–33.
Williams, D.A., Horsburgh, K.J., Schultz, D.M., Hughes, C.W., 2019. Examination of generation mechanisms for an English channel meteotsunami: combining observations and modeling. J. Phys. Oceanogr. 49 (1), 103–120.
Yao, Y., He, F., Tang, Z., Liu, Z., Feb. 2018. A study of tsunami-like solitary wave transformation and run-up over fringing reefs. Ocean Eng. 149, 142–155.